Journal of Molecular Catalysis A: Chemical 310 (2009) 75–82

Contents lists available at ScienceDirect

Journal of Molecular Catalysis A: Chemical

journal homepage: www.elsevier.com/locate/molcata

On the modulation of N_2 activation from molecular orbitals viewpoint Triamidoamine-Mo complexes as case of study

Hugo Vázquez-Lima, Patricia Guadarrama*, Estrella Ramos, Serguei Fomine

Instituto de Investigaciones en Materiales, Universidad Nacional Autónoma de México, Apartado Postal 70-360, CU, Coyoacán, México DF 04510, Mexico

ARTICLE INFO

Article history:
Received 26 March 2009
Received in revised form 25 May 2009
Accepted 27 May 2009
Available online 6 June 2009

Keywords:
N_2 activation
Triamidoamine complexes
Electrophilicity index
Density Functional Theory

ABSTRACT

Simplified models (model A: $[(PhNCH_2CH_2)_3N]Mo$; model B: $[(PhNCH_2CH_2)_3N]Mo–N_2$) based on triamidoamine complexes were proposed to evaluate the electrostatic/orbital effects of the phenyl rings on complexation and reduction of N_2. The effect of systematic synchronized rotations (from 0° to 90°) of phenyl dihedral angles on the charge and/or orbital contribution of molybdenum to complex N_2 was studied by chemical descriptors like electrophilicity index (ω) and Mulliken charges. According with the results, there is a favorable modulation of the energy gap of interaction between $HOMO/SOMO_{modelA}$ and $LUMO/LUMO{+}1_{N2}$ corresponding to π-back-donation interaction. It is confirmed that phenyl rings not only work as steric walls but also affect the orbital interactions. In accordance with ω values, Model A behaves as nucleophile with respect to N_2. This observation is in agreement with the suggestion that back-donation governs the complex-N_2 interaction. The rotation of dihedral angles of model B also has an effect on the electrophilicity index, allowing modulation in reductive processes. Inductive effects were also assessed by the substituents CN, Br and NH_2 in *para* position on the phenyl rings. The best scenario for N_2 complexation and activation was obtained with $[(p\text{-}NH_2PhenylNCH_2CH_2)_3N]Mo$. The Density Functional Theory was used as theoretical framework.

1. Introduction

Industrially, ammonia production from hydrogen and molecular nitrogen N_2 takes place at 550 °C and 150–350 atm of pressure through the Haber–Bosch process, to produce up to hundred millions of tons of NH_3 per year, even though such drastic conditions are involved [1]. Many systems using transition metals have been developed for N_2 activation [2,3]; however, some of them only coordinate N_2 or even weaken the N–N bond but non-catalytic process is involved and the reduction to NH_3 is not achieved. The most successful models to improve the catalytic reduction of N_2 by abiotic means have been those reported by Schrock et al. [4,5], based on molybdenum triamidoamine complexes with voluminous aryl ligands directly attached (Fig. 1).

The best results in terms of N_2 reduction were observed when the sterical hindrances were maximized via substituents, preventing the formation of bimetallic complexes, presumably unreactive toward the N_2 reduction, and improving the solubility [6,7]. The catalyst $[(ArNCH_2CH_2)_3N]Mo(III)$, where Ar = hexa-isopropyl-terphenyl (HIPT) [8] (Fig. 1) was able to reduce N_2 at room temperature and 1 atm of pressure, with an efficiency around 63% [6].

After some experimental variations made on the Aryl part of the ligand, including more or less sterical hindrances, as well as different electronic environments, Schrock's group observed that such variations result in a significant decrease in the N_2 reduction efficiency (less than 9% of NH_3 in some cases), thus, the electronic and steric features of the HIPT seem to be "ideal" to carry out the N_2 reduction [4].

Since the publication of the catalytic cycle proposed by Schrock for the reduction of N_2, the thermodynamic evaluation to justify and even predict critical intermediates by the construction of energy profiles has been the most recurring issue theoretically addressed [9,10,11], taking advantage of the applicability of the Density Functional Theory (DFT) methodology [12]. Most of the approaches have made some kind of simplification on the $[(HIPTNCH_2CH_2)_3N]Mo$ molecule. The studies carried out by Reiher et al. have proved that in order to approximate the theoretical results to the experiment (N_2 and NH_3 coordination reactions) no simplification of the ligand should be done [12,13]. This idea is somewhat shared by the experimentalists [14].

Beyond the analysis of the whole catalytic cycle, in the present study we turn over the singular role of the aryl substituents on the

* Corresponding author.
E-mail address: patriciagua@correo.unam.mx (P. Guadarrama).

1381-1169/$ – see front matter © 2009 Elsevier B.V. All rights reserved.
doi:10.1016/j.molcata.2009.05.019

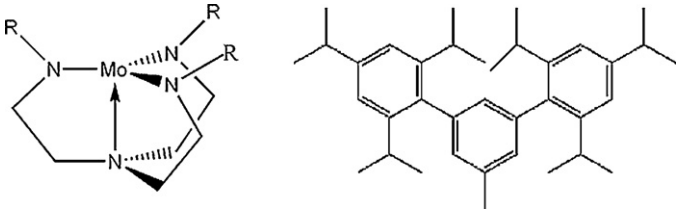

Fig. 1. Mo(III) complexes. R = aryl substituent.

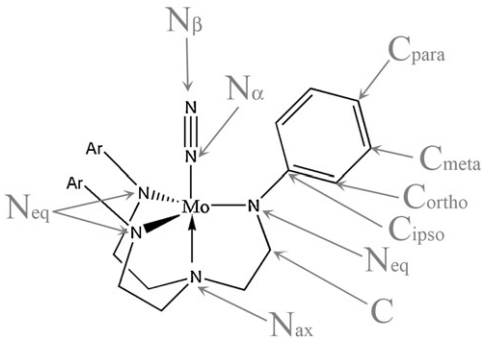

Fig. 2. Notation for triamidoamine ligands.

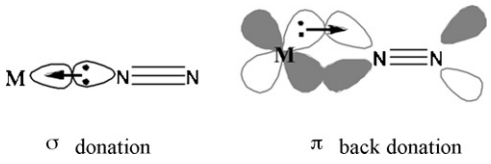

Fig. 3. Schematic representation of M–N electronic interaction.

reactivity of this kind of metal complexes towards the N_2 activation and reduction.

From the crystallographic data [15,16] summarized in Table 1 (see Fig. 2 for notation), among all the geometrical parameters, the dihedral angle Mo–N_{eq}–C_{ipso}–C_{ortho} of each intermediate in the catalytic cycle is one which exhibits marked variations along the cycle, indicating a relatively free rotation of the voluminous aryl substituents.

In the first step of the cycle (formation of [(HIPTNCH$_2$CH$_2$)$_3$N]Mo–N_2), simultaneous events of electron donation and back donation should take place, with the concomitant weakening of the N–N bond (Fig. 3).

Taking into account on the one hand the free-rotation of the aryl substituents and, on the other hand the electronic interactions involved in the first step to reduce N_2, the hypothesis to evaluate the contribution of aryl substituents was set forth as follows: If the manipulation of the aryl substituents (by systematic rotation of the dihedral angles Mo–N_{eq}–C_{ipso}–C_{ortho}) results in a favorable change in the interaction with N_2 from the electronic point of view, then sterical isolation is not their only role. The last consideration has been mentioned before by other authors [12,13,17] but it has not been systematically explored. Our hypothesis is that these aryl substituents might contribute to the electronic state of the Mo depending on the dihedral angle. If that is true, a favorable scenario of interaction could be found by systematic rotations of dihedral angles, which may be fixed by specific molecular templates (e.g. rigid dendritic scaffolds) to construct a nitrogen-reducer macromolecular catalyst.

In order to address the above hypothesis, restricted optimization calculations of simplified models of the [(HIPTNCH$_2$CH$_2$)$_3$N]Mo molecule were performed. The use of simplified models is necessary in the present study since some dihedral angles would not be accessible for sterical reasons.

It has been proposed that [(HIPTNCH$_2$CH$_2$)$_3$N]Mo is a highly delocalized system and population analysis to obtain localized charges does not describe properly any trend at all [17]. However, global descriptors of reactivity [18] such as electronic chemical potential (μ), chemical hardness (η) and the electrophilicity index (ω) defined by Parr et al. [19] consider the whole molecule. Particularly, relationships such as ω-dihedral angles, ω-energy profiles and ω-Diels-Alder reactions pairs have been estimated [20,21,22].

Thus, in this work μ, η and ω were calculated to rationalize the differences in the chemical environment when the aryl substituents are in different positions. Particularly the descriptor ω, as a measure of the energetic stabilization when a molecular system acquires additional electronic charge, would be useful to describe the interaction between N_2 and Mo-complex since electron transfer is entailed. A comparison between HIPT and phenyl as substituents was made in order to hint at the overall effect of the model simplification. Inductive effects due to some functional groups (NH_2, Br, CN) on reactivity were also analyzed. The DFT framework was used.

2. Computational details

2.1. Validation

In order to validate the method, full optimization of the crystallographic structure shown in Fig. 4 ([(HIPTNCH$_2$CH$_2$)$_3$N]Mo–N_2) was carried out at DFT level. The functionals BHandHLYP [23] and BP86 [24,25,26] with the restricted open shell formalism (RO) and the basis set LACVP* [27] with polarized functions on heavy atoms were used. Atomic sections were set, taking into account two fragments (differentiated by colors pink and blue in Fig. 4). All calculations were performed using the program Jaguar 6.5 [28].

The reproducibility of geometrical data was taken as a validation criterion [9,11,12], especially the N_α–N_β distance, directly related to the N_2 activation.

The functional BHandHLYP reproduced the N_α–N_β distance (difference of 0.05 Å) better than BP86 (difference 0.1 Å) with respect to the crystallographic structure. The discrepancy in the Mo–N_α distance was 0.1 Å in both cases. The functional BHandHLYP was

Table 1
Summary of crystallographic data of isolated intermediates from the Schrock catalytic cycle. Mo=[(HIPTNCH$_2$CH$_2$)$_3$N]Mo.

Mo oxidation state		–Mo–N_2 III	Mo–N=N– IV	Mo–N=NH IV	Mo–N=NH_2^+ VI	Mo≡N VI	Mo=NH^+ VI	Mo–NH_3^+ IV	Mo–NH_3 III
Distance (Å)	Mo–N_{ec}	1.978	2.030	2.010	1.954	2.003	1.944	1.948	2.003
	Mo–Na_x	2.188	2.241	2.228	2.236	2.395	2.286	2.147	2.205
	Mo–N_α	1.963	1.863	1.780	1.743	1.652	1.631	2.236	2.170
	N_α–N_β	1.061	1.156	1.302	1.304	–	–	–	–
Dihedral angle Mo–N_{ec}–C_{ipso}–C_{ortho}	67.38	−31.65	−32.23	69.11	34.06	67.88	74.02	64.26	
	69.14	−35.37	−33.47	71.54	34.81	70.77	74.77	69.02	
	70.83	−29.25	−39.47	73.20	35.29	72.07	82.07	72.95	

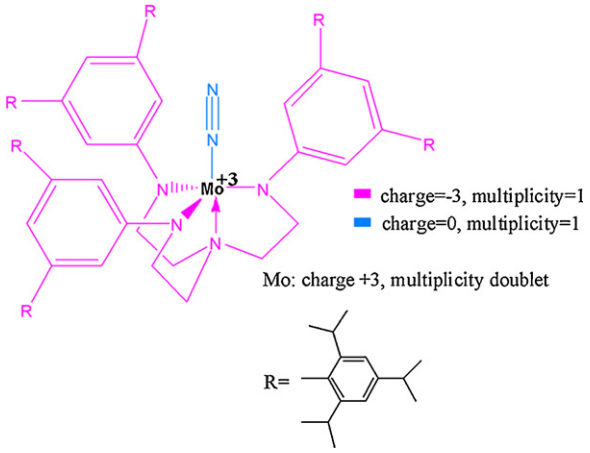

Fig. 4. N_2-triamidoamine complex of molybdenum.

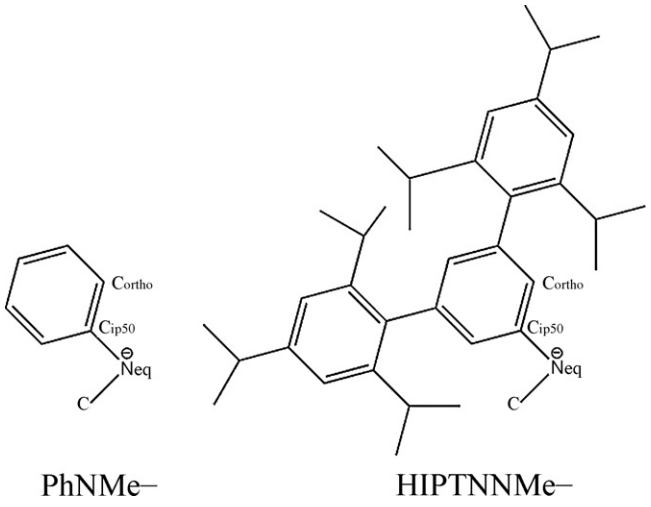

Fig. 5. Fragments models of $HIPTNMe^-$ and $PhNMe^-$.

chosen for further calculations since it gave a better reproduction of the most important distance in terms of activation.

The half and half approximation incorporated in BHandHLYP is the highlight of the functional, with no empirical parameters and involving only a rigorous ab initio formula called adiabatic connection [29].

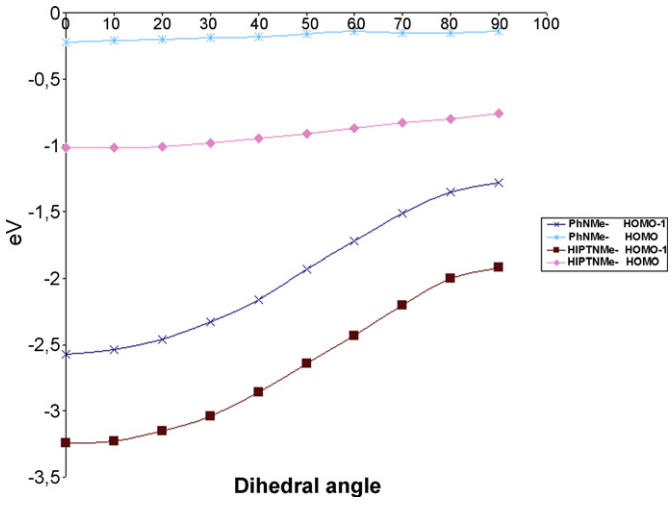

Graphic 1. MO energies from $HIPTNMe^-$ and $PhNMe^-$ fragments through systematic rotations.

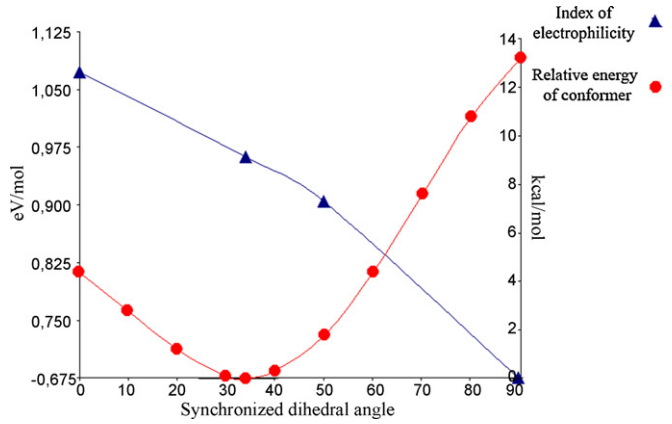

Graphic 2. Energies and ω of Model A through systematic rotations.

As it was reported before for this complex [16], the doublet multiplicity is favored over the quartet. At the level of theory used in this study (ROBHandHLYP/ LACVP*), the doublet was indeed more stable by 5.08 kcal.

All the calculations were carried out in vacuum since all the experiments with triamidoamine complexes occur in heptanes (dielectric constant = 1.92).

2.2. Models for the comparison of HIPT versus phenyl

In order to underline the similitude between R = HIPT and R = Phenyl regarding the role they play in $[(RNCH_2CH_2)_3N]Mo$ we have carried out calculations of molecular orbitals (MO) at ROBHandHLYP/6-31** + level of theory. $HIPTNMe^-$ and $PhNMe^-$ fragments were optimized with different restrictions of the dihedral angle $C–N_{eq}–C_{ipso}–C_{ortho}$ (see Fig. 5). This angle has been rotated from 0° to 90° with increments of 10° for both models.

2.3. Simplified molecular models

Once the simplification of the model was justified (see Section 3) models A and B (N_2-complexed) shown in Figs. 6 and 7 were constructed and fully optimized at ROBHandHLYP/LACVP* level of theory (DFT frontier orbitals and energies are shown below).

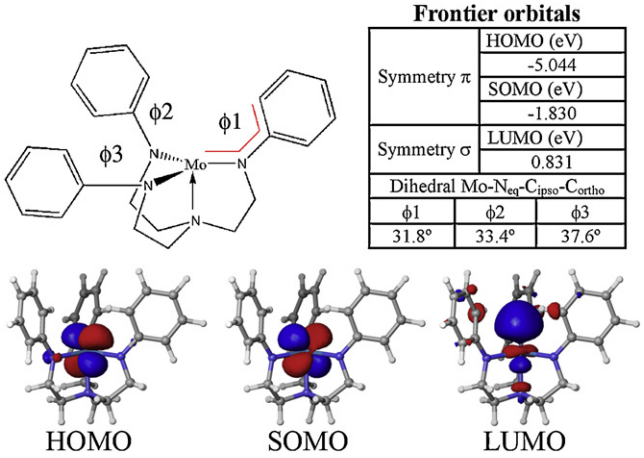

Frontier orbitals

Symmetry π	HOMO (eV)
	-5.044
	SOMO (eV)
	-1.830
Symmetry σ	LUMO (eV)
	0.831

Dihedral Mo-N_{eq}-C_{ipso}-C_{ortho}		
ϕ1	ϕ2	ϕ3
31.8°	33.4°	37.6°

Fig. 6. Simplified model A fully optimized at ROBHandHLYP/LACVP* level.

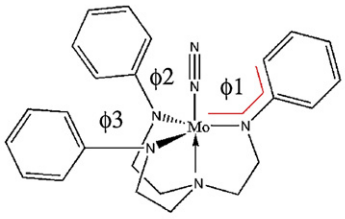

Frontier orbitals

Symmetry π	HOMO (eV)
	-5.880
	SOMO (eV)
	-2.223
	LUMO (eV)
	0.965

Dihedral Mo-N_{eq}-C_{ipso}-C_{ortho}		
ϕ1	ϕ2	ϕ3
45.0°	49.3°	50.2°

Distances	
Mo-N_α	N_α-N_β
2.080	1.103

Angle Mo-N_α-N_β
178.78°

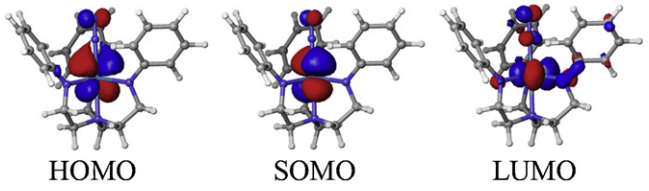

Fig. 7. Simplified model B (N_2 complexed) fully optimized at ROBHandHLYP/LACVP* level.

Systematic rotations on dihedral angles $\phi1$, $\phi2$ and $\phi3$ were carried out in a synchronized fashion and the reactivity towards the N_2 activation, by means of global descriptors like Mulliken charges [30] and the index of electrophilicity (ω), was estimated. In case of model B, interaction energies with N_2 was also calculated along with each rotation of dihedral angles.

Systematic rotations were made as follows: The three dihedral angles $\phi1$, $\phi2$ and $\phi3$ were rotated in a synchronized mode, from 0° (notation: 0° 0° 0°) to 90° (notation: 90° 90° 90°) with increments of 10°. Once the structures were manually generated, geometry optimizations were carried out at ROBHandHLYP/LACVP*, maintaining the restrictions on the dihedral angles.

This methodology was also applied to models containing *para* substituents NH_2, Br and CN on phenyl to evaluate the inductive effect of electron-donating and electron-withdrawing groups (Fig. 8).

3. Results and discussion

Regarding the crystallographic data, very small differences in the Mo–N and N_α–N_β distances (0.009 and 0.001 Å, respectively) were observed when the optimized model B was compared with the whole HIPT–Mo complex; thus, the simplified models were considered reliable for further calculations.

The energy of the two electron pairs of each equatorial nitrogen (N_{eq}) determines the availability of electrons on the metal center. According to MO theory, the molybdenum atom in a C_3 environment can only accept 10 electrons (e^-) from the $3N_{eq}$. These electrons come from an ensemble of 2 e^- π and 2e^- σ for each N_{eq} giving a total of 12 e^-. The remaining 2 e^- are left without any interaction for symmetry reasons (see support information). The energy of these 10 e^- is governed, among other factors by the dihedral angle Mo–N_{eq}–C_{ipso}–C_{ortho} (or C–N_{eq}–C_{ipso}–C_{ortho} for small fragments).

In Fig. 9 the MO graphical representations of these two electron pairs are shown for models $PhNMe^-$ and $HIPTNMe^-$ in selected dihedral angles. It can be noticed for model $PhNMe^-$ that while the delocalization of the π e^- decreases, the delocalization of the σ e^- increases. However the energy change for the π e^- is smaller (+0.08 eV going from 0° to 90°) than for the σ e^- (+1.29 eV going from 0° to 90°). This result shows that major tuning of the electronic environment of the molybdenum can be achieved by

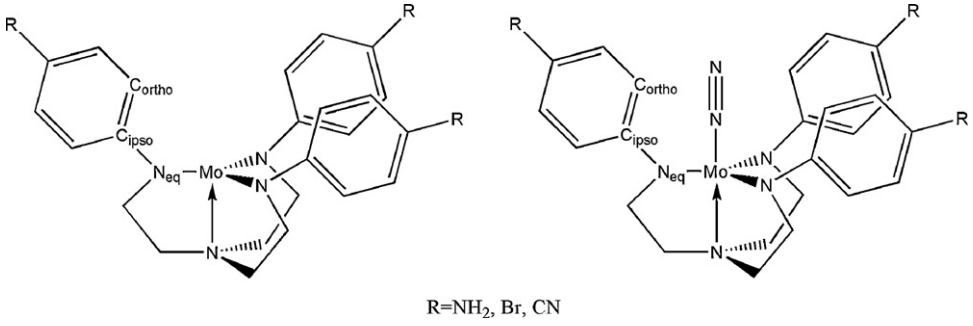

Fig. 8. Simplified models with inductive groups.

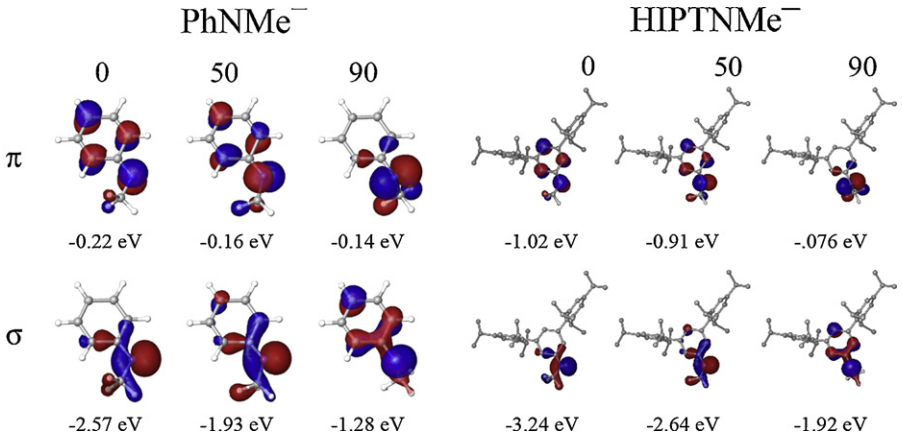

Fig. 9. Molecular orbitals of fragment models $HIPTNMe^-$ and $PhNMe^-$ in conformations 0°, 50° and 90°.

Table 2
Energy variation of frontier orbitals through systematic rotations of fragments $PhNMe^-$ and $HIPTNMe^-$ (values in eV).

Dihedral	PhNMe–		HIPTNMe–	
	HOMO-1	HOMO	HOMO-1	HOMO
0° (Fully optimized)	−2.57	−0.22	−3.24	−1.02
10°	−2.54	−0.21	−3.23	−1.02
20°	−2.46	−0.20	−3.15	−1.01
30°	−2.33	−0.19	−3.04	−0.98
40°	−2.16	−0.18	−2.86	−0.95
50°	−1.93	−0.16	−2.64	−0.91
60°	−1.72	−0.14	−2.43	−0.87
70°	−1.51	−0.15	−2.20	−0.83
80°	−1.35	−0.15	−2.00	−0.80
90°	−1.28	−0.14	−1.92	−0.76

σ electrons rather than by π electrons. The same behaviour is observed for model $HIPTNMe^-$; the energy changes of π and σ orbitals are + 0.26 eV and + 1.32 eV respectively from 0° to 90°. These data shown the agreement in the tendency of energy modification through rotations of both $HIPTNMe^-$ and $PhNMe^-$ fragments (see Graphic 1).

Table 2 contains MO energies data of $HIPTNMe^-$ and $PhNMe^-$ models optimised with restricted dihedral angle. After full optimisations of $PhNMe^-$and $HIPTNMe^-$ without restrictions the dihedral angle $C–N_{eq}–C_{ipso}–C_{ortho}$ became 0°. Although differences exist between HIPT and Phenyl frontier orbital energies, the tendency through the systematic rotation remains. According to this, it would be expected that the complexation energies of the actual $[(HIPTNCH_2CH_2)_3N]Mo$ and the simplified model $[(PhCH_2CH_2)_3N]Mo$ with N_2 follow the same tendency.

One of the reasons why the N_2 has poor reactivity is the very large energy gap between frontier orbitals (HOMO-LUMO), which renders the molecule resistant to electron transfer redox processes and Lewis acid-base reactions [31].The frontier MO of N_2 were calculated at RBHandHLYP/LACVP* level of theory (Fig. 10). For symmetry reasons, the HOMO and degenerated LUMO and LUMO + 1 (anti-bonding) of N_2 with σ and π symmetry respectively could interact with the LUMO and HOMO and SOMO (Single Occupied Molecular Orbital) of A (see Fig. 6).

Considering the N_2 energy gap, it is clear that an increase in energy of the HOMO and SOMO of A would improve the interaction with the LUMO of N_2, while a decrement in its LUMO energy (more negative) could also help it to interact with the HOMO of N_2.

The modulation of these deltas of energy was explored by synchronized rotations of the dihedral angles ϕ1, ϕ2 and ϕ3. The results are shown in Table 3 where an increment in the energy of the HOMO and SOMO of A can be observed as the dihedral angles are modified; which is accompanied by some destabilization with respect to the fully optimized A (13 kcal/mol maximum). Considering the LUMO and LUMO + 1 energy of N_2, moving ϕ1, ϕ2 and ϕ3 of A toward 90° brings the energy of the orbitals closer, improving

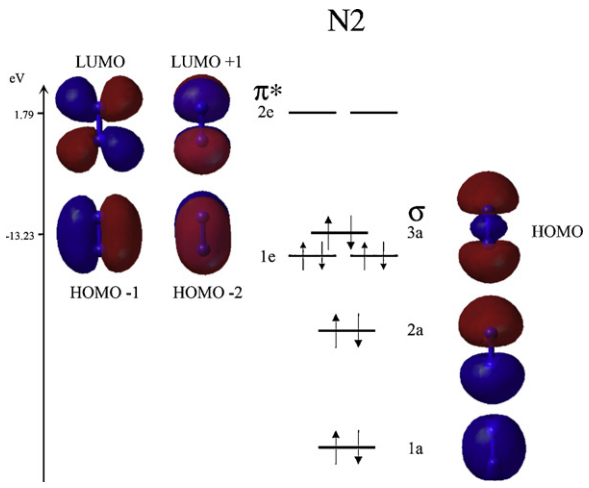

Fig. 10. DFT frontier orbitals of N_2.

the back-donation interaction (see Fig. 3), at expense of complex destabilization.

On the other hand, the energy of the LUMO of A shows a small but perceptible decrement toward 0° or 90°, which is also a desirable event in terms of the σ donation interaction. The electrophilicity index defined as:

$$\omega = \frac{\mu^2}{2\eta} \quad \text{Eq. (3) (see Ref. [19])}$$

where η (chemical hardness) = 1/2($I - A$), μ (electronic chemical potential) = 1/2($I + A$), I = ionisation potential and A = electron affinity, was calculated for all the conformers of model A.

It was used the adiabatic approximation for ionisation potentials ($I_{adiabatic}$) and electron affinities ($A_{adiabatic}$), calculated as the difference between the energies of the reference molecule (N electron system) and the corresponding N − 1 or N + 1 electron systems, respectively. In Table 4 are shown the adiabatic parameters and electrophilicity indexes corresponding to the synchronized rotations at the extremes; 0° 0° 0° and 90° 90° 90°, passing through 50° 50° 50°. The behavior of relative energies and ω values of the conformers is illustrated in Graphic 2. The same descriptors were calculated for N_2 at the same level of theory ($A_{adiabatic}$ = −3.310 eV, $I_{adiabatic}$ = 15.450 eV, ω = 1.964 eV).

When the electrophilic character is analyzed by means of ω, it can be noticed that N_2 has a larger value than model A (free or with any restriction). This indicates that nitrogen would take electrons from the complex upon coordination, suggesting that back-bonding through HOMO and SOMO of A governs the interaction rather than the electron-donation from nitrogen to A. The $\Delta\omega$ between A and N_2 vary from 0.891 to 1.292 eV, which is a similar difference to $\Delta\omega$ of polar Diels-Alder reactions [20,21]. It is important to mention that,

Table 3
Energy variation of frontier orbitals and relative energy through systematic dihedral rotations of Model A.

$\phi1, \phi2, \phi3$ rotation	ε_{HOMO} (eV)	ε_{SOMO} (eV)	ε_{LUMO} (eV)	Relative energy to fully optimizaed (kcal/mol)
Fully optimized	−5.044	−1.830	0.831	0
0° 0° 0°	−5.149	−2.002	0.759	4.4
10° 10° 10°	−5.150	−2.001	0.782	2.8
20° 20° 20°	−5.101	−1.934	0.806	1.2
30° 30° 30°	−5.044	−1.861	0.820	0.1
40° 40° 40°	−4.774	−1.773	0.830	0.3
50° 50° 50°	−4.940	−1.709	0.795	1.8
60° 60° 60°	−4.885	−1.637	0.769	4.4
70° 70° 70°	−4.827	−1.579	0.730	7.6
80° 80° 80°	−4.763	−1.487	0.715	10.8
90° 90° 90°	−4.701	−1.444	0.712	13.2

Table 4
Variations of adiabatic *A*, *I* and ω through systematic dihedral rotations (values in eV).

$\phi1, \phi2, \phi3$ rotation	Model A			Para-NH_2 (without N_2)			Para-Br (without N_2)			Para-CN (without N_2)		
	$A_{adiabatic}$	$I_{adiabatic}$	ω	$A_{adiabatic}$	$I_{adiabatic}$	ω	$A_{adiabatic}$	$I_{adiabatic}$	ω	$A_{adiabatic}$	$I_{adiabatic}$	ω
Free	−0.150	4.279	0.962	−0.454	3.740	0.643	0.395	4.900	1.556	0.792	5.392	2.078
0° 0° 0°	−0.087	4.550	1.073	−0.380	4.171	0.789	0.408	5.152	1.629	0.993	5.537	2.346
50° 50° 50°	−0.212	4.215	0.905	−0.775	3.603	0.457	0.246	4.791	1.395	0.705	5.182	1.935
90° 90° 90°	−0.529	4.032	0.672	−0.877	3.694	0.434	−0.058	4.519	1.087	0.488	4.935	1.653
$\phi1, \phi2, \phi3$ rotation	Model B			Para-NH2 (N_2-complexed)			Para-Br (N_2-complexed)			Para-CN (N_2-complexed)		
	$A_{adiabatic}$	$I_{adiabatic}$	ω	$A_{adiabatic}$	$I_{adiabatic}$	ω	$A_{adiabatic}$	$I_{adiabatic}$	ω	$A_{adiabatic}$	$I_{adiabatic}$	ω
Free	0.707	4.748	1.840	0.435	4.350	1.462	1.211	5.152	2.569	1.831	5.556	3.662
0° 0° 0°	0.953	4.889	2.168	0.887	4.393	1.988	1.507	5.295	3.054	1.998	5.759	4.000
50° 50° 50°	0.670	4.784	1.808	0.434	4.321	1.455	1.171	5.189	2.517	1.681	5.675	3.387
90° 90° 90°	0.267	4.504	1.343	0.024	4.034	1.027	0.753	4.888	1.924	1.272	5.331	2.685

Table 5
Interaction energies with N_2 (kcal/mol).[a,b]

$\phi1, \phi2, \phi3$ rotation	Hydrogen	Para-NH_2	Para-Br	Para-CN
0° 0° 0°	−12.4	−11.8	−12.8	−11.6
10° 10° 10°	−13.4			
20° 20° 20°	−16.2			
30° 30° 30°	−18.0			
40° 40° 40°	−19.9			
50° 50° 50°	−21.5	−27.8	−22.6	−29.3
60° 60° 60°	−22.7			
70° 70° 70°	−24.1			
80° 80° 80°	−25.4			
90° 90° 90°	−26.4	−27.5	−26.9	−26.0

[a] Obtained form the rest of $E_{Uncomplexd}$ and E_{N2} to $E_{N2\text{-complexed}}$.
[b] Values of fully optimized interaction energies: hydrogen, −20.8; *para*-NH_2, −23.7; *para*-Br, −21.6; *para*-CN, −23.1

even smaller variations of the ω index (eg. 0.06–0.04) than those observed in Table 4 have been successfully related with biological activity [32].

In this analogy to the Diels-Alder reaction, N_2 acts as electrophile and model A as nucleophile. A better nucleophile would improve this interaction and such quality is modulated through dihedral angles of A, lowering its values of ω and producing the largest $\Delta\omega$. Both, the largest interaction energy between N_2 and model A as well as the highest energy values of HOMO and SOMO (improving the interaction with the LUMO of N_2) are obtained in conformation 90° 90° 90° (Table 5). The dihedral angle around 90°, as a likely conformation to improve the interaction between the Mo-complex and N_2, could be fixed if a molecular environment is carefully chosen, for instance by rigid dendritic scaffolds [32].

The results obtained for model A reinforce the fact that aromatic substituents like HIPT do not only play the role of steric walls but they also tune the reactivity through the modulation of frontier MO energy towards N_2.

Once the N_2 has interacted with the model A, model B is attained (Fig. 7). The interaction energies were calculated, as a function of the synchronized rotation from 0° 0° 0° to 90° 90° 90°. These data are presented in Table 5:

The interaction energy corresponding to the fully optimized structure (without restrictions) can be located between those obtained for conformers 40° 40° 40° and 50° 50° 50°. A further increment in the interaction energy occurs as the 90° 90° 90° conformer is approached; however, the main increments are observed for conformations 0° 0° 0° to 50° 50° 50°.

Mulliken charges were calculated for models A and B, the whole HIPT–Mo complex and the crystallographic structure (see support information). The variation on the charges were too small to be significant.

Inductive effects due to substituents in *para* position of phenyl rings from model A was addressed. The aim was to search for an improvement in the HOMO-LUMO gap due to the groups NH_2, Br and CN. Table 6 shows the orbital energies corresponding to the rotations at the extremes; 0° 0° 0° and 90° 90° 90°, passing through 50° 50° 50°.

The electron-withdrawing effect of CN and, in less extent of Br, decreases the energies of the HOMO and SOMO (with π-symmetry) in regard to model A without substituents, moving them away to interact with the LUMO and LUMO + 1 of N_2. This observation can be associated with the experiment where the *p*-BrHIPT ligand produced lower yields of NH_3 than HIPT with no substituents [4]. The LUMO energy in these two cases moved in the desired direction to improve the σ-interaction. On the other hand, the electron-donating group NH_2 favors the π-back donation since there is an increment around 0.6 eV (∼14 kcal) in energy of the HOMO, comparing with model A without substituents. The σ-interaction in this case is not favored.

The energy of LUMO in the presence of CN, Br or NH_2 shows only slight differences along the synchronized rotations. Thus, as before, the back bonding to N_2 is more affected.

In order to relate the values of ω obtained for *para* substituted derivates of model A with the results of Molecular Orbitals, some considerations should be made. As we mentioned before, the criterion to designate as electrophile or nucleophile a molecule in a pair depends on ω values. The molecule with the higher value would attract electrons and the molecule with lower value would give them. For most of the cases presented in Table 4, N_2 always have higher value of ω with respect to model A.

Exceptions are 0° 0° 0° and free conformations for *para*-CN molecules. In these two special cases the electrons will flow from N_2 to molybdenum complex, which means that the prefer interaction in these particular cases is σ (HOMO from N_2 and LUMO from

Table 6
Frontier molecular orbitals energy of model A with different substituents. Evaluation of inductive effects. (Values in eV).

p-Substituent	CN			Br			NH_2		
$\phi1, \phi2, \phi3$ rotation	0°	50°	90°	0°	50°	90°	0°	50°	90°
HOMO (eV)	−6.15	−5.84	−5.66	−5.65	−5.43	−5.173	−4.55	−4.32	−4.341
SOMO (eV)	−3.206	−2.705	−2.594	−2.67	−2.39	−2.084	−1.85	−1.33	−1.244
LUMO (eV)	−0.260	−0.152	−0.216	0.166	0.25	0.267	0.88	0.092	0.932

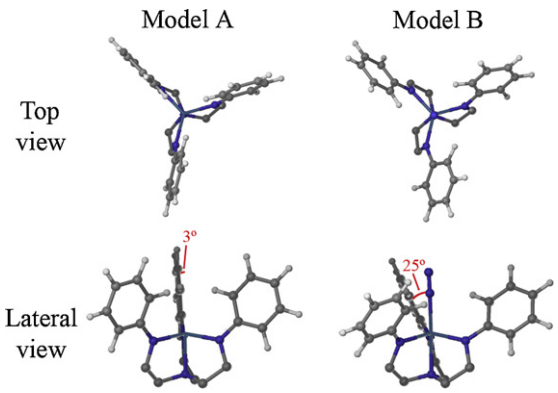

Fig. 11. Deviation of the perpendicular plane in models A and B.

complex). But considering $\Delta\omega$ values, varying from −0.311 to 0.382 in the *para*-CN series, we will regard the interaction as similar to frontier-orbital controlled Diels-Alder Reaction.

The *para*-Br series is located in the middle of polar and frontier orbital controlled, varying $\Delta\omega$ from −0.335 to −0.877, meanwhile the *para*-NH_2 series is the most polar of the four analyzed, varying $\Delta\omega$ from −1.175 to −1.530.

The values of interaction energy in the *para*-substitued complexes does not follow clear trends. For instance, we would expect that conformation 0° 0° 0° from *para*-CN complex have higher values of interaction energy due to the fact that 0° 0° 0° has the smallest gap of $LUMO_{complex}$–$HOMO_{N2}$ of all complexes and the $\Delta\omega$ is small. However, the interaction energy is the smallest value of Table 5. This is attributed to repulsive effects (see Fig. 11). When the conformation 0° 0° 0° of model A (without N_2) is achieved, the planes C–N_{eq}–C_{ipso} are align practically perpendicular to the plane formed by the 3 N_{eq} and molybdenum, with a small deviation of 3°. This place the π orbitals of each N_{eq} in the plane of the empty d_{x2-y2} and d_{xy} from molybdenum. Upon coordination of N_2, there is some repulsion between the phenyl rings and the N_2 which takes out of the perpendicular position the planes of C–N_{eq}–C_{ipso} forming an angle of 65° instead of 90°. This effect lowers the interaction of π orbitals from N_{eq} with empty d_{x2-y2} and d_{xy} orbitals from molybdenum.

We have seen that complexes with *para*-electron donor groups enhance its effect in conformation 90° 90° 90° and *para*-electron withdrawing groups should enhance its effect in 0° 0° 0° conformation but, as we can not access to this enhancement in the case of *para*-electron withdrawing groups due to repulsive effects, we will consider again the *para*-NH_2 and conformations near 90° 90° 90° as the best scenario.

Considering the forthcoming reduction of N_2 once it has interacted with Mo-complex, the descriptor ω was calculated for model B and its *para*-NH_2, Br, CN substitutions to evaluate the electrophilicity (see Table 4).

As seen from the ω values, the electron-withdrawing nature of Br and CN is reflected as a larger electrophilicity index, which is convenient in terms of eventual reduction processes, but is unfavorable in terms of N_2 complexation (as shown before). When the substituent is NH_2, the electrophilic character decreases making the reduction process more difficult but the N_2 complexation is favored.

Taking into account the "proton-catalyzed reduction" mechanism proposed by Yandulov and Schrock [15] for $[(HIPTNCH_2CH_2)_3N]Mo–N_2$ reduction (see Refs. [14,17]) the first step that most likely should occur is the addition of H^+. This would render the most nucleophilic complex as the best candidate for the task. Nucleophilicity is related to a low electrophilicity index [20,21], so complexes with the lowest value of ω would be preferred. Analyzing the molecules N_2-complexed in Table 4, those with *para*-NH_2 have the lower values of ω and among them, the conformation 90° 90° 90° has the lowest. This would be the selected candidate to activate N_2 towards its reduction.

All the above information points to a complex with *para*-NH_2 substitution and a molecular framework orienting the Mo–N_{eq}–C_{ipso}–C_{ortho} around 90° for a better N_2 activation.

The presence of donor substituents like NH_2 (or OH) are associated with an electron-rich metal center capable to make the step of reduction of N_2 the crucial step of the cycle [33].

In order to find the molecular framework capable to enclose the best scenarios found before, a first evaluation of an hydrophobic rigid channel model, necessary for the diffusion of NH_3, is in

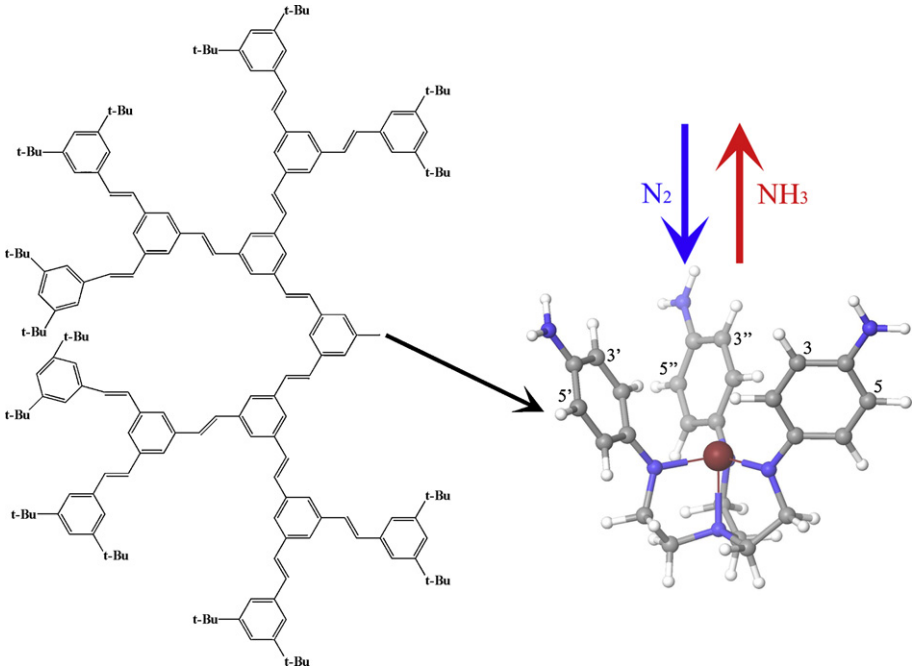

Fig. 12. Hydrophobic channel model, including the optimal simplified model.

progress. It includes dendrons of poly(phenylene vinylene) of first generation [34], as is shown in Fig. 12, attached to the positions 3, 5, 3′, 5′, 3″ and 5″ of the simplified model.

4. Conclusions

Simplified models A and B were used to evaluate the electrostatic/orbital effects of the phenyl rings position on the steps of N_2 complexation and reduction. Even though the molecules associated to Model A have not been isolated [14,35]; from such model was possible to analyze the back-bonding from its separate components achieving the rationalization of the effects that govern such process.

Synchronized rotations of the dihedral angles Mo–N_{ec}–C_{ipso}–C_{ortho} were carried out from 0° (notation: 0° 0° 0°) to 90° (notation: 90° 90° 90°) with gradual increments of 10°. The evaluation of the complexation ability towards N_2 for each conformer was made trough HOMO–LUMO energies and electrophilicity index (ω). Our results show that there is a favorable modulation of the interaction's energy gap between $HOMO/SOMO_{modelA}$ and $LUMO/LUMO+1_{N2}$ corresponding to π-back-donation interaction. Conformations close to 90° 90° 90° dihedral angles improve this interaction with some cost in complex destabilization. With the obtained results it is confirmed that phenyl rings not only work as steric walls but also affect the orbital interaction. The electrophilicity index of model A along the rotations was always lower than for N_2, placing the model A (Mo-complex) as electron-donor (nucleophile) with respect to N_2. This observation agrees with the idea that back-donation governs the complex-N_2 interaction.

Once the N_2 has been complexed (model B), the rotation of dihedral angles also has an effect on the electrophilicity index, allowing modulation in reductive processes.

Finally, inductive effects were assessed by the incorporation of the substituents CN, Br and NH_2 in *para* position on the phenyl rings. The best scenario for N_2 complexation and activation was obtained with [(*p*-NH_2PhenylN$CH_2CH_2)_3$N]Mo with Mo–N_{eq}–C_{ipso}–C_{ortho} dihedral angles of around 90°.

Acknowledgement

This research was carried out with the support of grant IN-100906 from DGAPA to the purchase of software and hardware. We acknowledge the support of *DGSCA*, UNAM, for using *supercomputer KanBalam.*

Appendix A. Supplementary data

Supplementary data associated with this article can be found, in the online version, at doi:10.1016/j.molcata.2009.05.019.

References

[1] V. Smil, Enriching the Earth: Fritz Haber, Carl Bosch, and the Transformation of World Food Production; MIT Press: Cambridge, MA, 2004.
[2] F. Studt, F. Tuczek, J. Comput. Chem. 27 (2006) 1278–1291.
[3] H.-J. Himmel, M. Reiher, Angew. Chem. Int. Ed. 45 (2006) 6264–6288.
[4] V. Ritleng, D.V. Yandulov, W.W. Weare, R.R. Schrock, A.S. Hock, W.M. Davis, J. Am. Chem. Soc. 126 (2004) 6150–6163.
[5] R.R. Schrock, Acc. Chem. Res. 38 (2005) 955–962.
[6] D.V. Yandulov, R.R. Schrock, Science 301 (2003) 76–78.
[7] G.E. Greco, R.R. Schrock, Inorg. Chem. 40 (2001) 3861–3878.
[8] D.V. Yandulov, R.R. Schrock, J. Am. Chem. Soc. 124 (2002) 6252–6253.
[9] Z. Cao, Z. Zhou, H. Wan, Q. Zhang, Int. J. Quantum Chem. 103 (2005) 344–353.
[10] K. Mersmann, K.H. Horn, N. Bolres, N. Lehnert, F. Studt, F. Paulat, G. Peters, I. Ivanovic-Burmazovic, R. van Eldik, F. Tuczek, Inorg. Chem. 44 (2005) 3031–3045.
[11] F. Studt, F. Tuczek, Angew. Chem. Int. Ed. 44 (2005) 5639–5642.
[12] B. Le Guennic, B. Kirchner, M. Reiher, Chem. Eur. J. 11 (2005) 7448–7460.
[13] M. Reiher, B. Le Guennic, B. Kirchner, Inorg. Chem. 44 (2005) 9640–9642.
[14] R.R. Schrock, Angew. Chem. Int. Ed. 47 (2008) 5512–5522.
[15] D.V. Yandulov, R.R. Schrock, Inorg. Chem. 44 (2005) 1103–1117.
[16] D.V. Yandulov, R.R. Schrock, A.L. Rheingold, C. Ceccarelli, W.M. Davis, Inorg. Chem. 42 (2003) 796–813.
[17] S. Schenk, B. Le Guennic, B. Kirchner, M. Reiher, Inorg. Chem. 47 (2008) 3634–3650.
[18] H. Chermette, J. Comput. Chem. 20 (1999) 129–154.
[19] R.G. Parr, L.V. Szentpaly, S. Liu, J. Am. Chem. Soc. 121 (1999) 1922–1924.
[20] P.K. Chattaraj, U. Sarkar, D.R. Roy, Chem. Rev. 106 (2006) 2065–2091.
[21] L.R. Domingo, M.J. Aurrell, P. Pérez, R. Contreras, Tetrahedron 58 (2002) 4417–4423.
[22] R. Parthasarathi, J. Padmanabhan, V. Subramanian, B. Maiti, P.K. Chattaraj, J. Phys. Chem. A 107 (2003) 10346–10352.
[23] C. Lee, W. Yang, R. G. Parr, Phys. Rev. B 37 (1988) 785–789; implemented as described in B. Miehlich, A. Savin, H. Stoll, H. Preuss, Chem. Phys. Lett. 157 (1989) 200–206.
[24] J.P. Perdew, A. Zunger, Phys. Rev. B 23 (1981) 5048–5079.
[25] J.P. Perdew, Phys. Rev. B 33 (1986) 8822–8824.
[26] A.D. Becke, Phys. Rev. A 38 (1988) 3098–3100.
[27] P.J. Hay, W.R. Wadt, J. Chem. Phys. 82 (1985) 270–283, and 299-310.
[28] Jaguar, version 6.5, Schrödinger, LLC, New York, NY, 2006.
[29] A.D. Becke, J. Chem. Phys. 98 (1993) 5648–5652.
[30] R.S. Mulliken, J. Chem. Phys. 23 (1955) 1833–1840.
[31] R.G. Pearson, Chemical Hardness: Applications from Molecules to Solids, Wiley–VCH, Germany, 1997.
[32] R. Parthasarathi, V. Subramanian, D.R. Roy, P.K. Chattaraj, Bioorg. Med. Chem. 12 (2004) 5533–5543.
[33] S. Schenk, M. Reiher, Inorg. Chem. 48 (2009) 1638–1648.
[34] S.K. Deb, T.M. Maddux, L. Yu, J. Am. Chem. Soc. 119 (1997) 9079–9080.
[35] W.W. Weare, C. Dai, M.J. Byrnes, J.M. Chin, R.R. Schrock, Proc. Natl. Acad. Sci. U.S.A. 103 (2006) 17099–17106.